International Journal of Computational Methods and Experimental Measurements
Vol. 12, No. 3, September, 2024, pp. 227-235
Journal homepage: http://iieta.org/journals/ijcmem

Finite Element Analysis of the Effect of Carbon Nanotube Content on the Compressive Properties of Zirconia Nanocomposites

Iman Zaidan Alshih Yahya, Hasan Mahmood Kaedhi, Emad Toma Karash*, Waleed Mohammed Najm

Mechanical Technology Department, Technical Institute of Mosul, Northern Technical University, Mosul 41000, Iraq

Corresponding Author Email: emadbane2007@ntu.edu.iq

https://doi.org/10.18280/ijcmem.120304

Received: 9 July 2024
Revised: 3 September 2024
Accepted: 19 September 2024
Available online: 30 September 2024

Keywords:
zirconia nanotube, simulations, mechanical properties, bending load, compressive load, ceramic

ABSTRACT

This work continues the assessment of the application of carbon nanotubes (CNTs) mixed with zirconia (ZrO_2). The study examined the compressive, bending, and bond strengths of samples containing and lacking carbon nanotubes. Zirconia carbon nanotubes (ZrO_2) in the concentrations of 0.00 %, 0.01 %, 0.02 %, 0.03 %, 0.04 %, and 0.05 % were the subjects of six mixtures whose resistance was measured. The results were analyzed using the finite element method with the ANSYS 15.0 program. ANSYS 15.0 software is used to analyze compressive and bending loads as well as the conventional zirconia model. Showcase the advantages of moderately utilizing carbon nanotubes. Zirconia's mechanical properties can be improved more effectively by mineral/chemical mixtures or fibers without the issues related to carbon nanotube dispersion. Provide evidence of the advantages of moderately utilizing carbon nanotubes. Without the issues related to carbon nanotube dispersion or the health hazards of handling Nanomaterials, zirconia's mechanical properties can be improved more effectively by mineral/chemical mixtures or fibers. The maximum and ideal load for the load was found to be 163.5 MPa, which was approved in all tests after the six models were finished with their designs in the ANSYS program. This was based on the von mises stress value and the maximum shear stress value less than the yield strength of the basic material used. After making numerous attempts, this load was selected by increasing the load by a specific percentage until it reached the ideal load, at which point the original model was able to support the load without experiencing any problems. The results of the ANSYS program were compared and examined, and they showed that the models' resistance to deformations, displacements, stresses, and various strains greatly increased when carbon nanotubes were added. By adding more carbon nanotubes, those models will be more resilient to the strains and deformations caused by compressive loads. The deformation rate decreased by 60%, which was a very noticeable decrease, especially in the sixth model where the carbon percentage was 5%.

1. INTRODUCTION

Owing to their exceptional potential and distinct characteristics, ceramic matrix composites offer a new generation of technically advanced applications with exceptional efficiency. Thanks to their strength, light weight, and exceptional resistance to wear, ceramic matrix composites are a great class of materials for use in great tribological applications, aerospace engineering (think hot structures), and automotive applications (think oxygen sensors and brake systems) [1-5].

Furthermore, ceramic materials have a strong reputation for being chemically inert, resistant to corrosion, strong, and thermally stable, which makes them ideal for applications that involve exposure to high temperatures or harsh environmental conditions. Low density ceramic materials with high wear and break resistance are needed in related industries like metallurgy and chemical to use them in cutting-edge applications [6-8]. Well-known biomaterials are ceramics based on the simultaneous presence of diopside ($CaMg(SiO_3)_2$) and wollastonite ($CaSiO_3$). The majority of the experiences are related to glass-ceramics from the regulated crystallization of glasses with B_2O_3, Na_2O, CaF2, and P_2O_5 additives that belong to the CaO-MgO-SiO2 system [9-11]. However, recent studies have shown the high bioactivity and biocompatibility of ceramics based only on the two silicate phases (in particular, based on eutectic point of the pseudo binary $CaSiO_2$-$CaMg(SiO_3)_2$ system [12]. The additives may cause the formation of additional phases, such as fluorapatite [11]. One of the most extensively studied and technologically resilient ceramic materials utilized in numerous applications are ZrO_2-based nanocomposites. Highly ionic conductivity, low density, chemical inertness, good wear resistance, high mechanical strength, and stability at elevated temperatures are just a few of the significant properties of ZrO_2 that have made it widely applicable in a variety of difficult structural, tribological, and multifunctional applications [13, 14]. Common uses are made to withstand challenging conditions and to meet the growing

global demand for clean energy. This can be achieved directly through the use of electrochemical power generation, as in the case of solid oxide fuel cell (SOFC) devices, or indirectly through the use of engines' thermal barrier layer, which guarantees that customers will be able to purchase inexpensive electricity because of the motor's high efficiency [15]. Further significant uses are in the domain of dental implants and load-bearing prostheses [16], where mechanical characteristics are crucial [17]. The first significant advancement in the synthesis and characterization of various structures containing zirconia nanotubes (ZNTs) was reported in 1997 [18]. Single-walled Zirconia nanotubes (SWZNT) have been synthesized and characterized using a variety of techniques, including hydrothermal treatments [19], the sol-gel method [20], anodization [21], bottom-up synthesis by impregnation [22], template-assisted depositions [23], and others. Numerous experimental studies [18, 24-26]. Determined a number of ZNT's physical, thermal, optical, electrical, and other properties. The scientific communities have been very interested in carbon nanotubes (CNTs) since their discovery [27], as evidenced by [28, 29]. These days, it is possible to produce large amounts of carbon nanotubes through the pyrolysis of hydrocarbons [30] or arc discharge [31]. Efficient growth of carbon nanotubes in terms of length, diameter, and straightness is crucial for prospective uses as well as in-depth property characterization. The direct pyrolysis of hydrocarbon gas to create insulated carbon nanotubes could be one new technological advancement. Using atomic force microscopy or transmission electron microscopy, numerous studies on physical properties, including flexural stiffness [32] and Young's modulus [33], have been conducted to date. Single-walled zirconia nanotube (SWZNT) properties have already been the subject of numerous simulations; however, these studies were limited to their physical and chemical aspects, including surface adsorption and diffusion, phonon dispersion, and atomic structures [34-42]. The ANSAS program will be used to run finite element method simulations on the mechanical properties (compressive loads, bending loads) of SWZNTS. For this study, ratios (Zirconia (ZrO_2) with carbon nanotubes in the concentrations of 0.00%, 0.01%, 0.02%, 0.03%, 0.04%, and 0.05%) will be used to create SWZNT structural models, which will then be subjected to various mechanical simulation forces. Lastly, an analysis and discussion of the deformations, stresses, and strains seen in SWZNT will be conducted.

2. MATERIALS USED

A total of twelve mathematical models were constructed, six for bending tests and six for compression tests. The first model was composed entirely of zirconia, while the other five models, as indicated in Table 1, included varying amounts of Nano carbon mixed with zirconia.

Table 1. Ratios of zirconia and carbon added to it in various models [43-47]

Model	Materials Friction Weight		Density, ρ, (g/mm^3)	Weight, g	Volume, mm^3	Volume Fractions	Modulus of Elasticity, E, (GPa)	Passion's Ratio	Tensile Strength MPa	Yield Strength MPa
Model - 1	Zirconia, (ZrO_2)		0.005832	3.5192	603.429	1.00	200	0.32	330	230
Model - 2	Zirconia & Carbon Nanotubes	Zirconia; (99%)	0.005832	2.6135	448.131	0.74	200	0.32	330	230
		Carbon Nanotubes; (1%)	0.00017	0.0264	155.288	0.26	1200	0.34	150000	102000
Model - 3	Zirconia & Carbon Nanotubes	Zirconia; (98%)	0.005832	2.0700	354.931	0.59	200	0.32	330	230
		Carbon Nanotubes; (2%)	0.00017	0.0422	248.494	0.41	1200	0.34	150000	102000
Model - 4	Zirconia & Carbon Nanotubes	Zirconia; (97%)	0.005832	1.7101	293.229	0.49	200	0.32	330	230
		Carbon Nanotubes; (3%)	0.00017	0.0529	311.171	0.51	1200	0.34	150000	102000
Model - 5	Zirconia & Carbon Nanotubes	Zirconia; (96%)	0.005832	1.4484	248.362	0.41	200	0.32	330	230
		Carbon Nanotubes; (4%)	0.00017	0.0604	355.012	0.59	1200	0.34	150000	102000
Model - 6	Zirconia & Carbon Nanotubes	Zirconia; (95%)	0.005832	1.3167	225.772	0.36	200	0.32	330	230
		Carbon Nanotubes; (5%)	0.00017	0.0693	407.647	0.64	1200	0.34	150000	102000

Table 2. The mechanical characteristics of composite materials produced by the software Mathcad 15

Models	Materials	K	E, GPa	G, GPa	μ
Model - 1	Zirconia, (ZrO_2)	-----	200	76	0.32
Model - 2	Zirconia & Carbon Nanotubes 74% - 26%	0.375	265	99.98	0.325
Model - 3	Zirconia & Carbon Nanotubes 59% - 41%	0.431	330.2	124.3	0.328
Model - 4	Zirconia & Carbon Nanotubes 0.49% - 0.51%	0.469	384.9	144.7	0.330
Model - 5	Zirconia & Carbon Nanotubes 41% - 59%	0.499	435.1	163.4	0.332
Model - 6	Zirconia & Carbon Nanotubes 26% - 74%	0.518	524	195.3	0.342

Table 3. Results of compression deformations, stresses and strain

Model	Maximum Comp. Deformations (mm)				Maximum Stresses Compressive (MPa)											Maximum Strains Compressive ($\mu\varepsilon$)							
	Ux	Uy	Uz	Usum	σ_x	σ_y	σ_z	τ_{xy}	τ_{yz}	τ_{xz}	σ_1	σ_2	σ_3	$\sigma_{int.}$	σ_{von}	ε_x	ε_y	ε_z	ε_{xy}	ε_{yz}	ε_{xz}	$\varepsilon_{int.}$	ε_{von}
M -1	0.0011	0.0011	0.0096	0.0967	142.61	143.19	304.31	15.00	80.78	92.29	99.76	143.20	347.15	247.40	230.02	0.00041	0.00040	0.00106	0.00203	0.00110	0.00122	0.00163	0.00115
M - 2	0.0008	0.0008	0.0073	0.0073	147.28	147.86	307.14	15.58	85.03	94.02	102.80	147.87	351.60	248.80	230.84	0.00032	0.00031	0.00079	0.00016	0.00085	0.00094	0.00124	0.00087
M - 3	0.0006	0.0006	0.0058	0.0059	150.14	150.73	308.86	15.71	85.92	95.06	104.67	150.74	354.32	249.65	231.33	0.00025	0.00024	0.00063	0.00012	0.00069	0.00076	0.00101	0.00070
M - 4	0.0005	0.0005	0.0050	0.0050	152.07	152.67	310.02	15.80	86.51	95.60	105.93	152.68	356.15	250.21	231.66	0.00022	0.00032	0.00054	0.00010	0.00059	0.00066	0.00086	0.00060
M - 5	0.0005	0.0005	0.0044	0.0044	254.03	154.63	311.18	15.88	87.11	96.45	107.21	154.64	357.99	250.78	231.99	0.00020	0.00019	0.00048	0.00009	0.00053	0.00059	0.00077	0.00053
M - 6	0.0004	0.0004	0.0037	0.0037	164.18	164.79	317.14	16.30	90.11	99.97	113.83	164.81	367.47	253.64	233.63	0.00017	0.00016	0.00039	0.00008	0.00046	0.00051	0.00065	0.00044

Table 2 shows the findings of the mechanical characteristics of the composite materials as determined by the Mathcad-15 program. Table 3 lists the models, codes, particular disciplines, element kinds, and load types applied by the ANSYS 15.0 program.

Fiber Composites with Random Orientation and Discontinuity Typically, in situations where short, discontinuous fibers with random orientation are employed, an expression known as the "rule-of-mixtures" for the elastic modulus can be employed, which is comparable to equations:

$$E_C = K.E_f.V_f + E_m.V_m \quad (1)$$

$$\mu_C = \mu_f + \mu_m \quad (2)$$

$$G_C = \frac{E_C}{2(1+\mu_C)} \quad (3)$$

where, E_C=Randomly Oriented Composite Modulus of Elasticity; K=Fibre Efficiency Parameter; E_f=Elastic Modulus of the Fibre; E_m=Elastic Modulus of the Matrix; V_f=Volume Fraction of the Fibre; V_m=Volume Fraction of the Matrix.

The fiber efficiency parameter (K) is dependent on the of (V_f & E_f/E_m ratio). Its magnitude will, of course, be less than unity; typically, it will be between 0.1 and 0.6. The fibers are uniformly and randomly distributed within a specific plane, which accounts for the value of (K=0.375) [48-50].

3. SIMULATING AND MODELING

3.1 Zirconia nanotube structures

For each of the six models, pressure screening specimens are created and prepared using composite materials in compliance with ASTM E9 standards. ANSYS software was utilized to conduct compression tests utilizing the finite element technique. For the purpose of compression testing, specimens measuring 8 mm in diameter and 12 mm in height were ready, as seen in Figure 1.

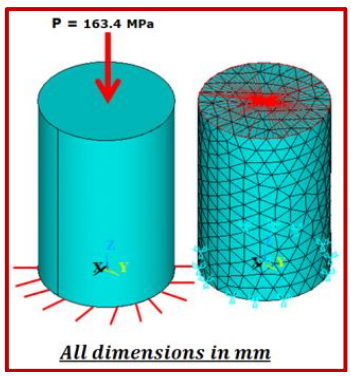

Figure 1. Schematic illustration of a compression test sample's dimensions [43]

4. RESULTS AND DISCUSSION

Table 3 and Figures 2-14 present the most significant findings from this investigation, which came from applying a compressive load of (163.4 MPa) to the models, (To find the load at which the first model collapses, the load was achieved through numerous attempts to load the model). By adding more of these materials to each model, the amounts of nanomaterial's in the various models were varied.

Table 3 and Figures 2-4, deformation, sum displacement, and displacement in direction - Z results, which were acquired by loading the six models, show a decline in its value, when comparing the five models to the first model in the following proportions: 24.6, 39.5, 48.1, 54.1, and 61.9%, respectively, with increasing ratios the Carbon Nanotubes in the models. Figure 5, which shows the normal stress in direction - Z results obtained by loading the six models, shows an increase in its value when comparing the five models to the first model in the following proportions: 0.93, 1.48, 1.87, 2.26, and 4.22%, respectively, as the ratio of carbon nanotubes in the models increases. Shear stress in direction-XZ results obtained by loading the six models are displayed in Figure 6, which demonstrate an increase in its value with increasing ratios of carbon nanotubes in the models. This increase is seen when comparing the five models to the first model in the following proportions: 1.87, 2.99, 3.75, 4.51, and 8.14%, respectively. Figure 7 present the shear stress in direction-ZY results obtained by loading the six models, showing an increase in its value with increasing ratios of carbon nanotubes in the models. The following proportions show this increase: 1.77, 2.84, 3.43, 4.27, and 7.86%, respectively, when comparing the five models to the first model. Figure 8 shows the intensity stress results of loading the six models, showing a marginal increase in its value as the models' carbon nanotube ratios rise. The percentages that demonstrate this increase between the first model and the five models are: 0.57, 0.91, 1.14, 1.77, and 2.52%, respectively.

The von Mises stress results obtained from loading the six models are shown in Figure 9, which indicates a very slight increase in their value as the models' proportions of carbon nanotubes increase. When comparing the five models to the first model, the following percentages demonstrate this increase: 0.36, 0.57, 0.72, 0.86, and 2.52%, respectively.

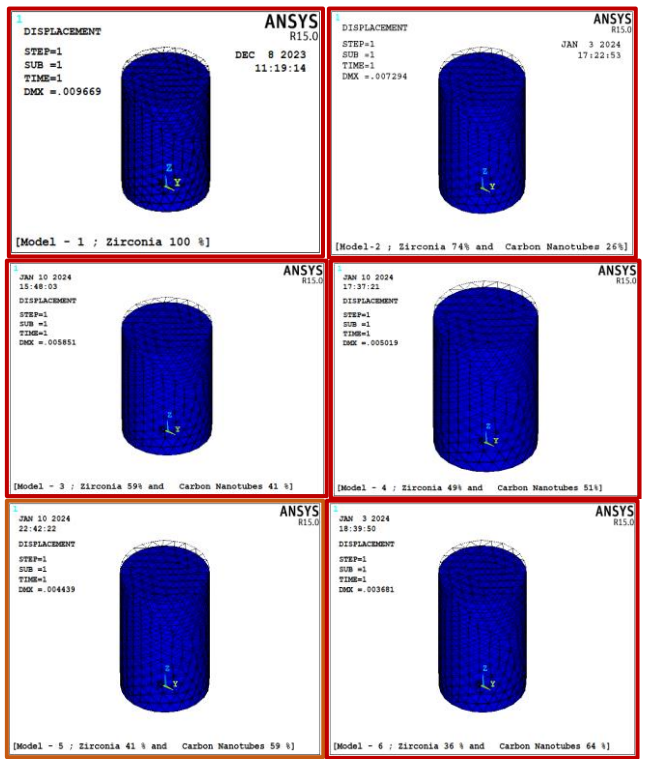

Figure 2. The results of the deformation for each model

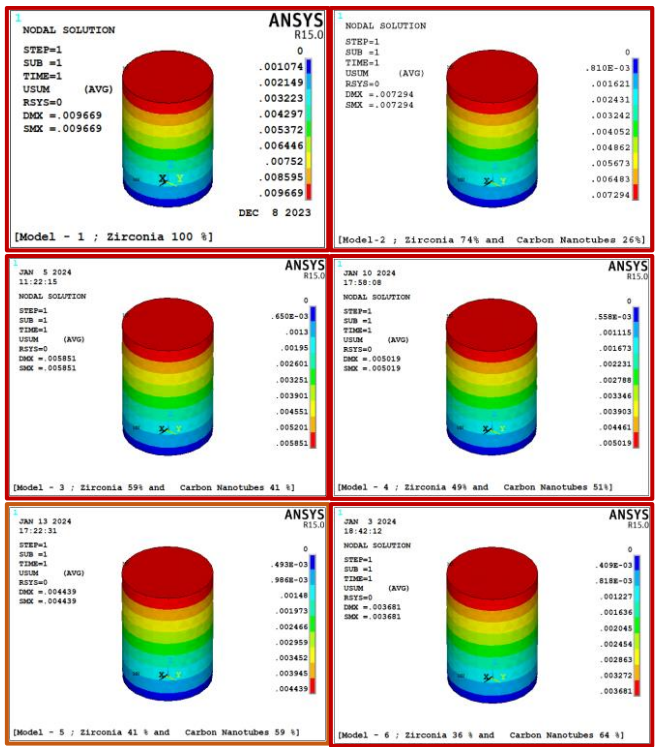

Figure 3. The results of the sum displacement (U_{sum}) for each model

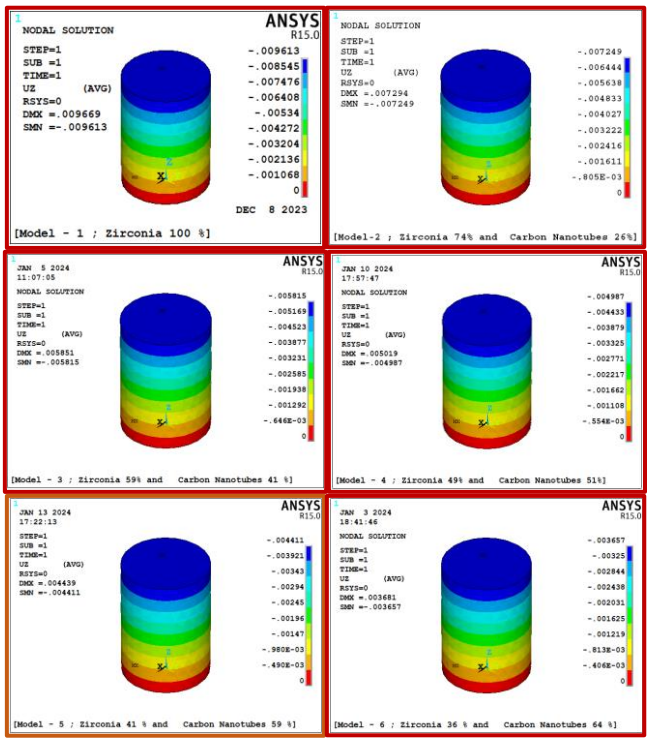

Figure 4. The results of the sum displacement (U_z) for each model

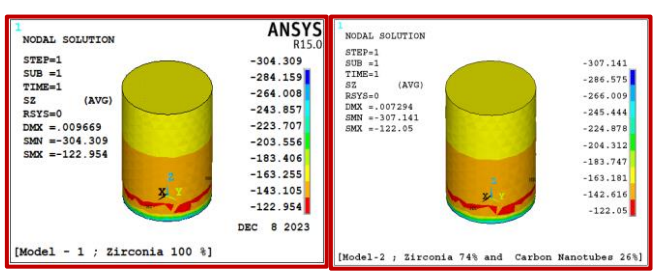

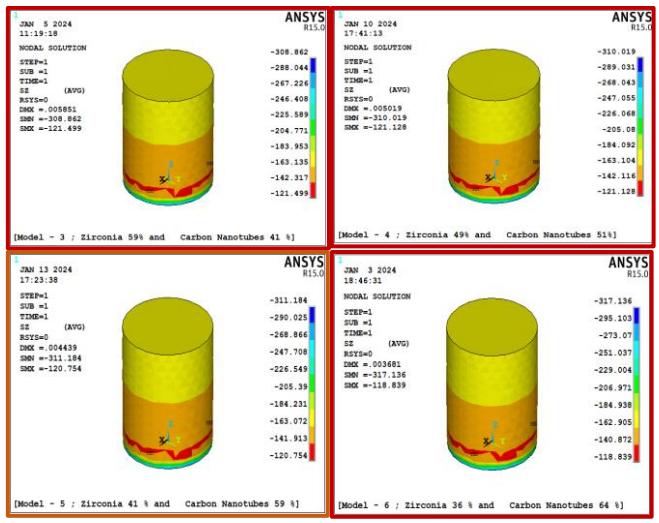

Figure 5. The results of the normal stress (σ_z) for each model

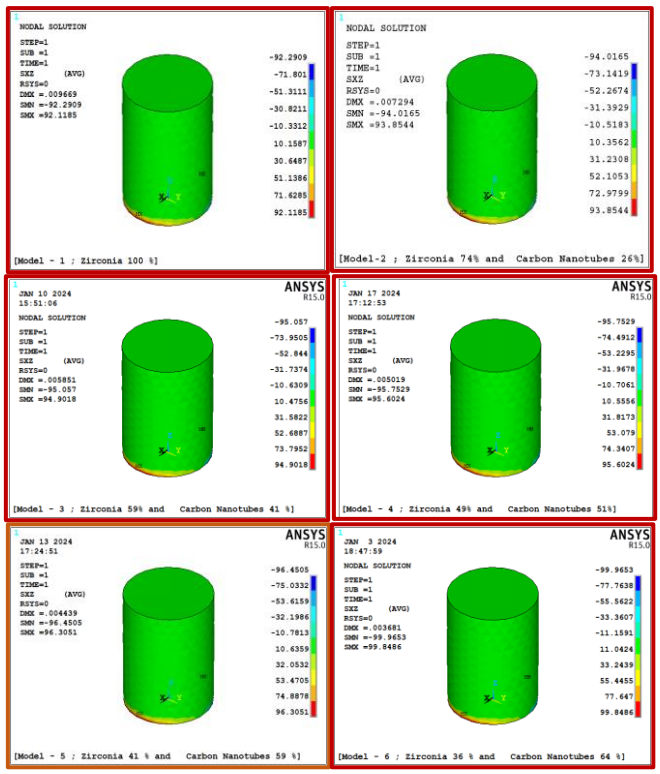

Figure 6. The results of the shear stress (τ_{xz}) for each model

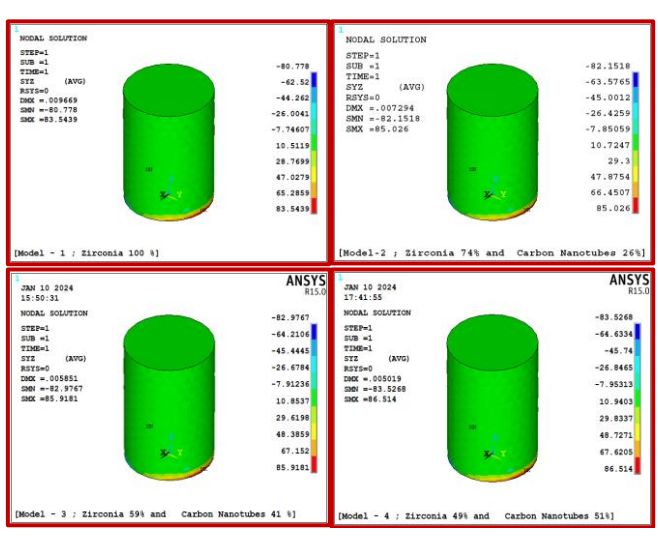

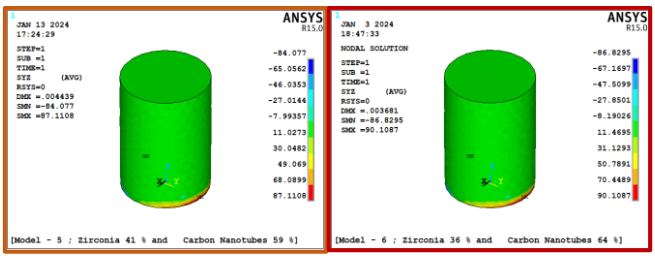

Figure 7. The results of the shear stress (τ_{yz}) for each model

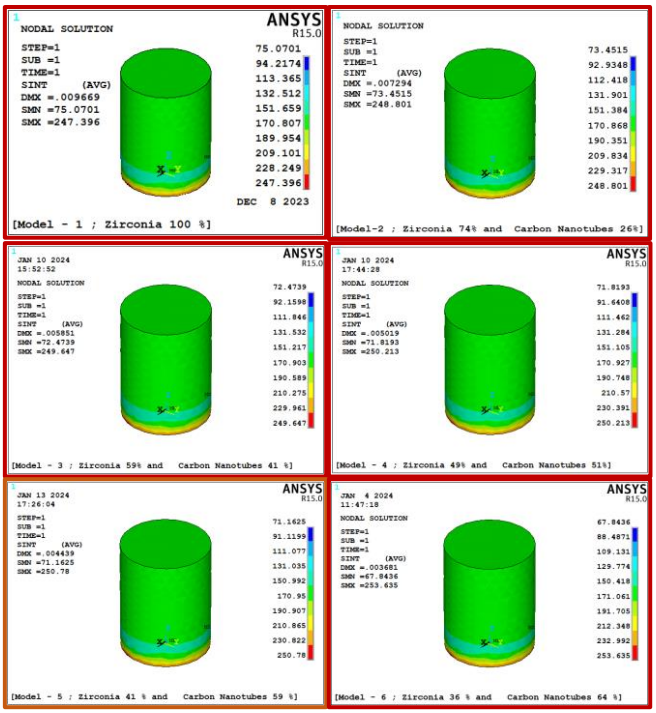

Figure 8. The results of the intensity stress ($\sigma_{int.}$) for each model

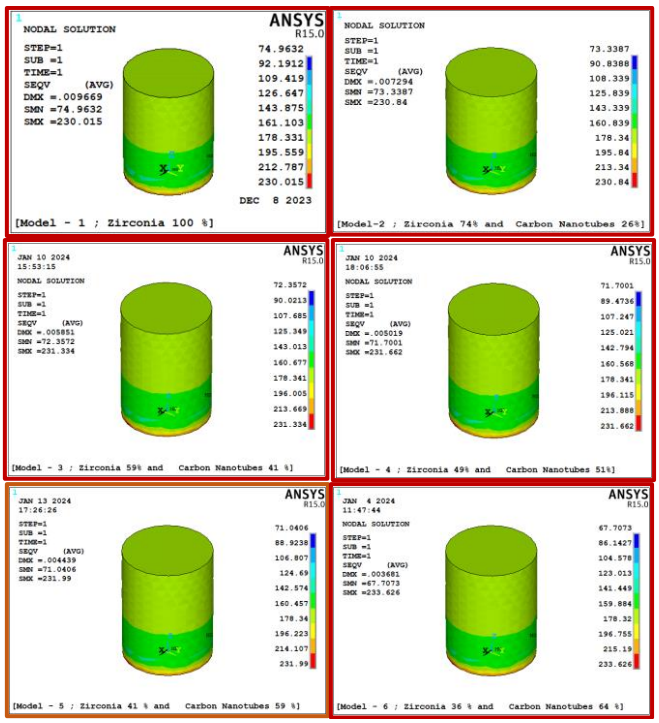

Figure 9. The results of the von mises stress (σ_{von}) for each model

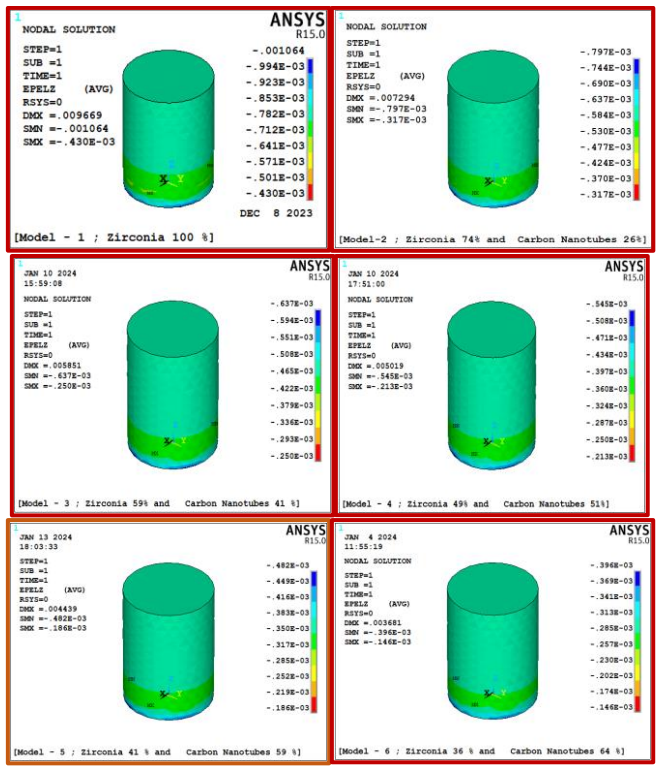

Figure 10. The results of the normal strain (ε_z) for each model

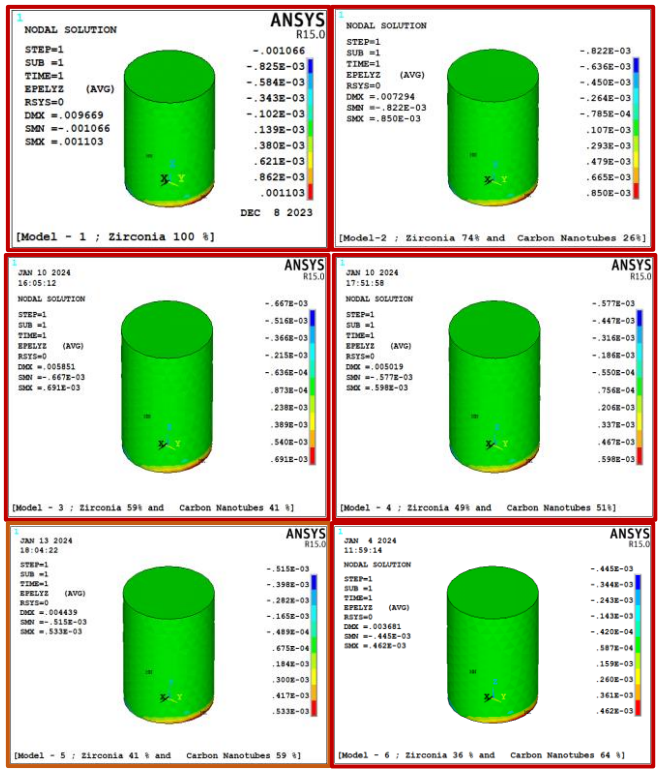

Figure 11. The results of the shear strain (ε_{yz}) for each model

Carbon nanotubes cause the crystalline structure of the material they are added to become rougher, which explains why stress results change very slightly when the content of carbon nanotubes is increased (^5% in most cases).

The results of loading the six models in Figure 10 show that there is a noticeable increase in strain in the direction of Z as the proportion of carbon nanotubes in the models increases. The following percentages demonstrate this increase when

comparing the five models to the first model: 25.47, 40.57, 49.06, 54.72, and 63.21%, respectively. Figure 11 shows the strain results in the direction of YZ that were obtained from loading the six models. It shows that the strain increases significantly as the proportion of carbon nanotubes in the models increases. The following percentages demonstrate this increase when comparing the five models to the first model: 22.73, 37.27, 46.36, 51.82, and 58.18%, respectively. Figure 12 shows the strain results in the XZ direction that were obtained after loading the six models. It demonstrates that when the amount of carbon nanotubes in the models rises, the strain increases noticeably. When comparing the five models to the first model, the following percentages show this increase: 22.95, 37.70, 45.90, 51.64, and 58.20%, respectively.

Figure 13 shows the intensity strain results that were obtained after the six models were loaded. It shows that there is a discernible increase in intensity strain with an increase in the number of carbon nanotubes in the models. The following percentages demonstrate this increase when comparing the five models to the first model: 23.93, 38.04, 47.24, 52.76, and 60.12%, in that order. Figure 14 shows the von Mises strain results that were obtained after loading the six models. It shows that the von Mises strain increases significantly with an increase in the number of carbon nanotubes in the models. The following percentages demonstrate this increase when comparing the five models to the first model: 24.35, 39.14, 47.83, 53.91, and 61.74%, respectively.

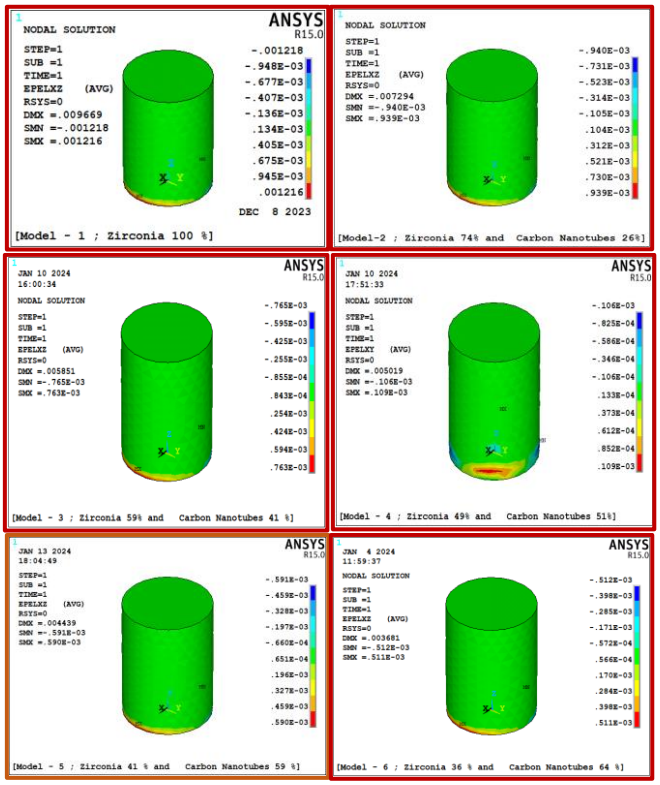

Figure 12. The results of the shear strain (ε_{xz}) for each model

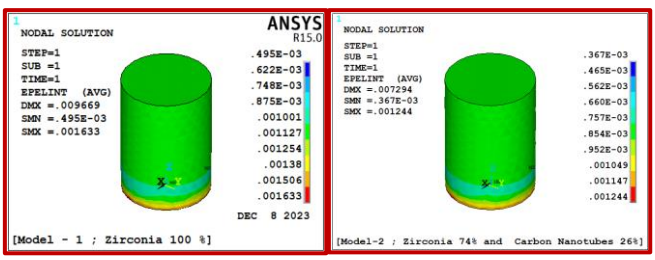

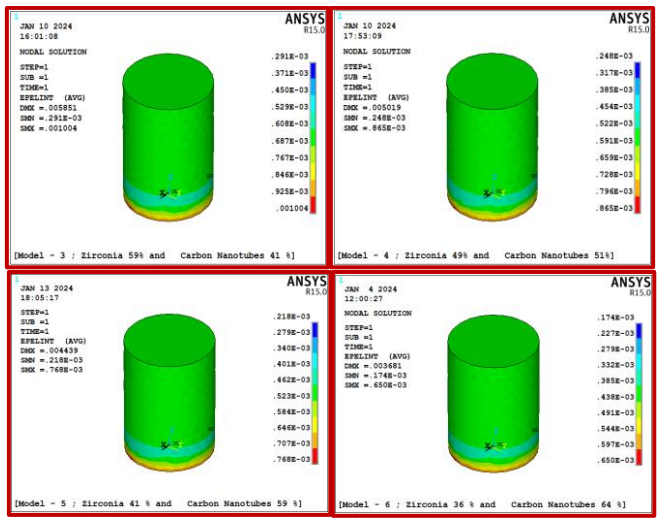

Figure 13. The results of the intensity strain ($\varepsilon_{int.}$) for each model

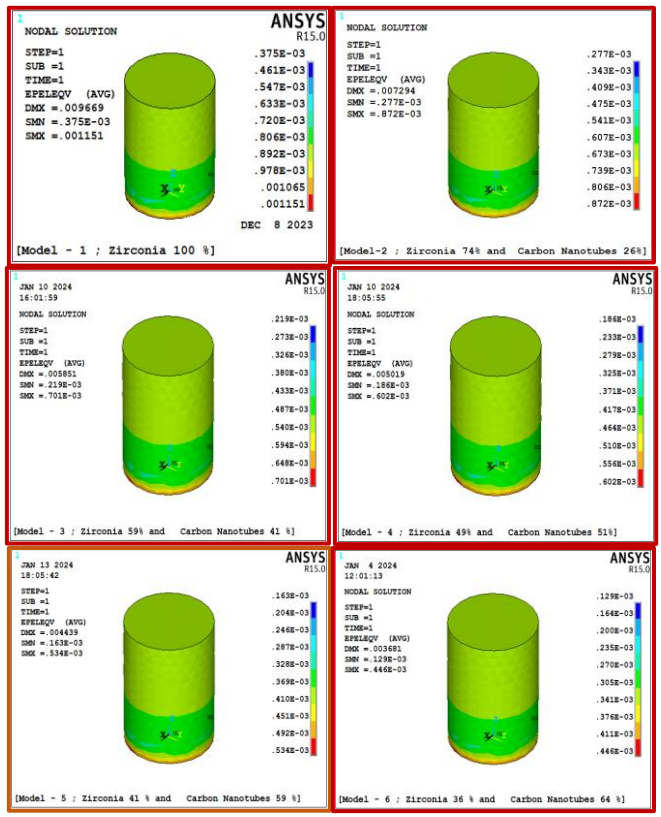

Figure 14. The results of the von mises strain (ε_{xvon}) for each model

The material to which the carbon nanotubes are added has a rougher crystal structure, which accounts for the very small change in the stresses results when compared to the high strains results.

5. CONCLUSIONS

The following was concluded from this theoretical study of composite materials composed of materials of different proportions by creating six models made of different materials, testing each model's compressive resistance, and comparing the results to one another in order to obtain materials with high

compressive resistance:

1. The results obtained show a significant decrease in deformation and deflection in the models, when the percentage of carbon nanotubes is increased at very high rates, which may reach 61.9% in the sixth model.

The primary cause of deformation sensing in carbon nanotube-polymer composites is the conductive carbon nanotube network's compressive strength inside the polymer matrices. Consequently, its deformation decreases due to the change in the mechanical deformation of the carbon nanotube network upon loading when its proportion in the material increases to a certain amount.

2. It is observed that applying a load of 163.5 MPa is the maximum optimal load for the models to bear this load without any failure occurring in them when using von Mises theory to compare the results obtained for the six models with the yield compressive strength of these materials.

3. It is also observed that the applied load is suitable for these models to function without failure when comparing the results with the theory of maximum shear stress.

6. FUTURE STUDIES

The researchers propose to create a number of mathematical models for different engineering materials, including aluminum alloys, composite materials, and magnesium alloys used in the medical field. They advise looking into how different loads in daily life affect engineering materials. withstand loads from impacts, twists, tensile and compression, torsion and fatigue, heat, and other sources. Using state-of-the-art engineering software, like the ANSYS program, carefully examine them to determine the deformations, stresses, and strains they experience during loading.

REFERENCES

[1] Lamnini, S., Pugliese, D., Baino, F. (2023). Zirconia-based ceramics reinforced by carbon nanotubes: A review with emphasis on mechanical properties. Ceramics, 6(3): 1705-1734. https://doi.org/10.3390/ceramics6030105

[2] Krupka, M., Kienzle, A. (2000). Fiber reinforced ceramic composite for brake discs. In Proceedings of the 18th Annual Brake Colloquium & Engineering Display, San Diego, CA, USA.

[3] Chan, K.F., Zaid, M.H.M., Mamat, M.S., Liza, S., Tanemura, M., Yaakob, Y. (2021). Recent developments in carbon nanotubes-reinforced ceramic matrix composites: A review on dispersion and densification techniques. Crystals, 11(5): 457. https://doi.org/10.3390/cryst11050457

[4] Hardwicke, C.U., Lau, Y.C. (2013). Advances in thermal spray coatings for gas turbines and energy generation: A review. Journal of Thermal Spray Technology, 22(5): 564-576. https://doi.org/10.1007/s11666-013-9904-0

[5] Cheng, Z., Liu, M. (2007). Characterization of sulfur poisoning of Ni-YSZ anodes for solid oxide fuel cells using in situ Raman microspectroscopy. Solid State Ionics, 178(13-14): 925-935. https://doi.org/10.1016/j.ssi.2007.04.004

[6] Fiocco, L., Ferroni, L., Gardin, C., Zavan, B., Secco, M., Matthews, S., Bernardo, E. (2016). Wollastonite-diopside glass-ceramic foams from supercritical carbon dioxide-assisted extrusion of a silicone resin and inorganic fillers. Journal of Non-Crystalline Solids, 443: 33-38. https://doi.org/10.1016/j.jnoncrysol.2016.04.012

[7] Li, F., Huang, X., Liu, J.X., Zhang, G.J. (2020). Sol-gel derived porous ultra-high temperature ceramics. Journal of Advanced Ceramics, 9: 1-16. https://doi.org/10.1007/s40145-019-0332-6

[8] Gorni, G., Velázquez, J.J., Mosa, J., Balda, R., Fernández, J., Durán, A., Castro, Y. (2018). Transparent glass-ceramics produced by sol-gel: A suitable alternative for photonic materials. Materials, 11(2): 212. https://doi.org/10.3390/ma11020212

[9] Agathopoulos, S., Tulyaganov, D.U., Ventura, J.M.G., Kannan, S., Karakassides, M.A., Ferreira, J.M.F. (2006). Formation of hydroxyapatite onto glasses of the CaO–MgO–SiO2 system with B2O3, Na2O, CaF2 and P2O5 additives. Biomaterials, 27(9): 1832-1840. https://doi.org/10.1016/j.biomaterials.2005.10.033

[10] Siriphannon, P., Kameshima, Y., Yasumori, A., Okada, K., Hayashi, S. (2002). Formation of hydroxyapatite on CaSiO3 powders in simulated body fluid. Journal of the European Ceramic Society, 22(4): 511-520. https://doi.org/10.1016/S0955-2219(01)00301-6

[11] Brawer, S.A., White, W.B. (1977). Raman spectroscopic investigation of the structure of silicate glasses (II). Soda-alkaline earth-alumina ternary and quaternary glasses. Journal of Non-Crystalline Solids, 23(2): 261-278. https://doi.org/10.1016/0022-3093(77)90009-6

[12] Gaddam, A., Tricot, G., Gołębiewski, P., Fernandes, H.R., Buczyński, R., Ferreira, J.M., Eckert, H. (2023). Structural organization of phase-separated bioactive glasses and the clustering of Si, P, B, Na and F atoms investigated by solid-state NMR and Monte Carlo simulations. Acta Materialia, 259: 119203. https://doi.org/10.1016/j.actamat.2023.119203

[13] Silvestre, J., Silvestre, N., De Brito, J. (2015). An overview on the improvement of mechanical properties of ceramics nanocomposites. Journal of Nanomaterials, 2015(1): 106494. https://doi.org/10.1155/2015/106494

[14] Kuntz, J.D., Zhan, G.D., Mukherjee, A.K. (2004). Nanocrystalline-matrix ceramic composites for improved fracture toughness. Mrs Bulletin, 29(1): 22-27. https://doi.org/10.1557/mrs2004.12

[15] Maiti, T.K., Majhi, J., Maiti, S.K., Singh, J., Dixit, P., Rohilla, T., Ghosh, S., Bhushan, S., Chattopadhyay, S. (2022). Zirconia-and ceria-based electrolytes for fuel cell applications: Critical advancements toward sustainable and clean energy production. Environmental Science and Pollution Research, 29(43): 64489-64512. https://doi.org/10.1007/s11356-022-22087-9

[16] Yin, L., Nakanishi, Y., Alao, A. R., Song, X.F., Abduo, J., Zhang, Y. (2017). A review of engineered zirconia surfaces in biomedical applications. Procedia Cirp, 65: 284-290. https://doi.org/10.1016/j.procir.2017.04.057

[17] Bistolfi, A., Ferracini, R., Lee, G.C., Mellano, D., Guidotti, C., Baino, F., Verné, E. (2021). Ceramic-on-ceramic catastrophic liner failure in total hip arthroplasty: Morphological and compositional analysis of fractured ceramic components. Ceramics International, 47(8): 11029-11036. https://doi.org/10.1016/j.ceramint.2020.12.225

[18] Tsuchiya, H., Macak, J.M., Taveira, L., Schmuki, P. (2005). Fabrication and characterization of smooth high

aspect ratio zirconia nanotubes. Chemical Physics Letters, 410(4-6): 188-191. https://doi.org/10.1016/j.cplett.2005.05.065
[19] Piticescu, R., Monty, C., Millers, D. (2005). Hydrothermal synthesis of nanostructured zirconia materials: Present state and future prospects. Sensors and Actuators B: Chemical, 109(1): 102-106. https://doi.org/10.1016/j.snb.2005.03.092
[20] Suciu, C., Gagea, L., Hoffmann, A.C., Mocean, M. (2006). Sol–gel production of zirconia nanoparticles with a new organic precursor. Chemical Engineering Science, 61(24): 7831-7835. https://doi.org/10.1016/j.ces.2006.09.006
[21] Wang, X., Zhao, J., Hou, X., He, Q., Tang, C. (2012). Catalytic activity of ZrO2 nanotube arrays prepared by anodization method. Journal of Nanomaterials, 2012(1): 409571. https://doi.org/10.1155/2012/409571
[22] Takenaka, S., Uwai, S., Ida, S., Matsune, H., Kishida, M. (2013). Bottom-up synthesis of titania and zirconia nanosheets and their composites with graphene. Chemistry Letters, 42(10): 1188-1190. https://doi.org/10.1246/cl.130587
[23] Patel, D., Bonova, L., Jeckell, Z., Barlaz, D.E., Chaudhuri, S., Krogstad, D.V., Ruzic, D.N. (2021). Deposition of zirconium oxide using atmospheric pressure plasma enhanced chemical vapor deposition with various precursors. Thin Solid Films, 733: 138815. https://doi.org/10.1016/j.tsf.2021.138815
[24] Ogihara, H., Sadakane, M., Nodasaka, Y., Ueda, W. (2006). Shape-controlled synthesis of ZrO2, Al2O3, and SiO2 nanotubes using carbon nanofibers as templates. Chemistry of Materials, 18(21): 4981-4983. https://doi.org/10.1021/cm061266t
[25] Wang, C., Wang, Y., Zhang, G., Chen, Y., Han, X., Liang, L., Xu, Y., Xu, L. (2020). Preparation of a novel transplant material, zirconium oxide (ZrO2) nanotubes, and characterizations research. Annals of Transplantation, 25: e924272-1. https://doi.org/10.12659/AOT.924272
[26] Nezhad, E.Z., Sarraf, M., Musharavati, F., Jaber, F., Wang, J.I., Hosseini, H.R.M., Bae, S., Chowdhury, M., So, H., Sukiman, N.L. (2022). Effect of zirconia nanotube coating on the hydrophilicity and mechanochemical behavior of zirconium for biomedical applications. Surfaces and Interfaces, 28: 101623. https://doi.org/10.1016/j.surfin.2021.101623
[27] Xie, S., Li, W., Pan, Z., Chang, B., Sun, L. (2000). Mechanical and physical properties on carbon nanotube. Journal of Physics and Chemistry of solids, 61(7): 1153-1158. https://doi.org/10.1016/S0022-3697(99)00376-5
[28] Wang, K., Gu, M., Wang, J.J., Qin, C., Dai, L. (2012). Functionalized carbon nanotube/polyacrylonitrile composite nanofibers: Fabrication and properties. Polymers for Advanced Technologies, 23(2): 262-271. https://doi.org/10.1002/pat.1866
[29] Jyoti, J., Basu, S., Singh, B.P., Dhakate, S.R. (2015). Superior mechanical and electrical properties of multiwall carbon nanotube reinforced acrylonitrile butadiene styrene high performance composites. Composites Part B: Engineering, 83: 58-65. https://doi.org/10.1016/j.compositesb.2015.08.055
[30] Ruoff, R.S., Qian, D., Liu, W.K. (2003). Mechanical properties of carbon nanotubes: Theoretical predictions and experimental measurements. Comptes rendus. Physique, 4(9): 993-1008. https://doi.org/10.1016/j.crhy.2003.08.001
[31] Miao, M., McDonnell, J., Vuckovic, L., Hawkins, S.C. (2010). Poisson's ratio and porosity of carbon nanotube dry-spun yarns. Carbon, 48(10): 2802-2811. https://doi.org/10.1016/j.carbon.2010.04.009
[32] Pandey, P., Dahiya, M. (2016). Carbon nanotubes: Types, methods of preparation and applications. Carbon, 1(4): 15-21.
[33] Kumar, K. (2022). Young's modulus of elasticity of carbon nanotube (CNT). International Journal of Mechanical Engineering, 7(7): 227-231.
[34] Muhammad, I.D., Awang, M. (2014). Modelling the interatomic potential of cubic zirconia. Applied Mechanics and Materials, 446: 151-157. https://doi.org/10.4028/www.scientific.net/AMM.446-447.151
[35] Karash, E.T., Slewa, M.Y., AL-Maula, B.H. (2023). State stress analysis of dental restoration materials using the ANSYS program. Journal of Composite & Advanced Materials/Revue des Composites et des Matériaux Avancés, 33(3): 183–192. https://doi.org/10.18280/rcma.330306
[36] Al-Gebory, L., Al-Zubaidi, A.B., Al-Tabbakh, A.A. (2020). Production of self-cleaning SiO2/CNT nanoparticles substituted cement mortar. Engineering and Technology Journal, 38(3A): 335-342. https://doi.org/10.30684/etj.v38i3A.349
[37] Sultan, J.N., Karash, E.T., Abdulrazzaq, T.K., Kassim, M.T.E. (2022). The effect of multi-walled carbon nanotubes additives on the tribological properties of austempered AISI 4340 steel. Journal Européen des Systèmes Automatisés, 55(3): 387-396. https://doi.org/10.18280/jesa.550311
[38] Guimaraes, L., Enyashin, A.., Seifert, G., Duarte, H.A. (2010). Structural, electronic, and mechanical properties of single-walled halloysite nanotube models. The Journal of Physical Chemistry C, 114(26): 11358-11363. https://doi.org/10.1021/jp100902e
[39] Meunier, M., Robertson, S. (2021). Materials studio 20th anniversary. Molecular Simulation, 47(7): 537-539. https://doi.org/10.1080/08927022.2021.1892093
[40] Bandura, A.V., Evarestov, R.A. (2012). Ab initio structure modeling of ZrO2 nanosheets and single-wall nanotubes. Computational Materials Science, 65: 395-405. https://doi.org/10.1016/j.commatsci.2012.08.001
[41] Yang, X., Li, H., Hu, M., Liu, Z., Wärnå, J., Cao, Y., Ahuja, R., Luo, W. (2018). Mechanical properties investigation on single-wall ZrO2 nanotubes: A finite element method with equivalent Poisson's ratio for chemical bonds. Physica E: Low-dimensional Systems and Nanostructures, 98: 23-28. https://doi.org/10.1016/j.physe.2017.10.005
[42] Muhammad, I.D., Awang, M., Mamat, O., Shaari, Z.B. (2014). First-principles calculations of the structural, mechanical and thermodynamics properties of cubic zirconia. World Journal of Nano Science and Engineering, 4(2): 97-103. https://doi.org/10.4236/wjnse.2014.42013
[43] Saleh, B., Jiang, J., Fathi, R., Xu, Q., Wang, L., Ma, A. (2020). Study of the microstructure and mechanical characteristics of AZ91–SiC p composites fabricated by stir casting. Archives of Civil and Mechanical Engineering, 20: 1-14. https://doi.org/10.1007/s43452-

020-00071-9
[44] Junior, S.A.R., Ferracane, J.L., Della Bona, A. (2008). Flexural strength and Weibull analysis of a microhybrid and a nanofill composite evaluated by 3-and 4-point bending tests. Dental Materials, 24(3): 426-431. https://doi.org/10.1016/j.dental.2007.05.013
[45] Jambagi, S.C., Kar, S., Brodard, P., Bandyopadhyay, P.P. (2016). Characteristics of plasma sprayed coatings produced from carbon nanotube doped ceramic powder feedstock. Materials & Design, 112: 392-401. https://doi.org/10.1016/j.matdes.2016.09.095
[46] Vandewalle, L. (2000). Recommendations of RILEM TC 162-TDF: Test and design methods for steel fibre reinforced concrete. Materials and Structures, 33: 75-81.
[47] Hou, P., Zhao, H., Ma, Z., Zhang, S., Li, J., Dong, X., Sun, Y., Zhu, Z. (2016). Influence of punch radius on elastic modulus of three-point bending tests. Advances in Mechanical Engineering, 8(5): 1687814016649116. https://doi.org/10.1177/1687814016649116
[48] Callister Jr, W.D., Rethwisch, D.G. (2020). Materials Science and Engineering: An Introduction. John Wiley & Sons.
[49] Krenchel, H. (1964). Fibre reinforcement. Copenhagen: Akademisk Forlag.
[50] Okagbare, G.O., Ikri, S.O. (2022). A review on the industrial applications and properties of fiber-reinforced and other polymeric composites. NIPES-Journal of Science and Technology Research, 4(2): 144-162. https://doi.org/10.37933/nipes.e/4.2.2022.15

NOMENCLATURE

δ	Deformed and unreformed
U_x	Component of the displacement (x-direction)
U_y	Component of the displacement (y-direction)
U_z	Component of the displacement (z-direction)
σ_x	Normal stress
τ_{xy}	Shear stress
τ_{xz}	Shear stress
$\sigma_{int.}$	Stress intensity
σ_{von}	Von mises stress
ε_x	Normal strain (x-direction)
ε_{xy}	Shear strain (xy-direction)
ε_{xz}	Shear strain (xz-direction)
ε_{first}	First principal elastic strain
ε_{third}	Third principal elastic strain
$\varepsilon_{intensty}$	Elatic strain intensty
ε_{von}	Von mises elatic strain

Greek symbols

E	Modulus of elacitisty
ρ	Density
G	Modulus of rigidity
μ	Passions ratio

Subscripts

SNC	Surface Nano Crystallization
Si	Silicone
Mn	Manganese
C	Carbon
Ni	Nickel
Ti	Titanium
Cr	Chrome
Fe	Iron